Research Article | Vol. 29, No. 7 / 29 March 2021 / Optics Express 11158
Optics EXPRESS

High-efficiency coupling of single quantum emitters into hole-tailored nanofibers

XIN WANG,[1] PENGFEI ZHANG,[1,2,3] GANG LI,[1,2] AND TIANCAI ZHANG[1,2,4]

[1] State Key Laboratory of Quantum Optics and Quantum Optics Devices, Institute of Opto-Electronics, Shanxi University, Taiyuan 030006, China
[2] Collaborative Innovation Center of Extreme Optics, Shanxi University, Taiyuan, Shanxi 030006, China
[3] zhangpengfei@sxu.edu.cn
[4] tczhang@sxu.edu.cn

Abstract: We propose a scheme to enhance the coupling efficiency of photons from a single quantum emitter into a hole-tailored nanofiber. The single quantum emitter is positioned inside a circular hole etched along the radial axis of the nanofiber. The coupling efficiency can be effectively enhanced and is twice as high as the case in which only an intact nanofiber without the hole is used. The effective enhancement independent of a cavity can avoid the selection of a single emitter for the specific wavelength, which means a broad operating wavelength range. Numerical simulations are performed to optimize the coupling efficiency by setting appropriate diameters of the nanofiber and the hole. The simulation results show that the coupling efficiency can reach 62.8% when the single quantum emitter with azimuthal polarization (x direction) is at a position 200 nm from the middle of the hole along the hole-axial direction. The diameters of the nanofiber and the hole are 800 nm and 400 nm, respectively, while the wavelength of the single quantum emitter is 852 nm. Hole-tailored nanofibers have a simple configuration and are easy to fabricate and integrate with other micro/nanophotonic structures; this fiber structure has wide application prospects in quantum information processing and quantum precision measurement.

1. Introduction

Recently, hybrid systems combining photonic devices and quantum emitters have attracted wide attention in quantum optics and quantum information processing [1,2] and have significant applications in areas such as strong light-matter interactions [3–5], single-photon sources [6], quantum logical gates [7,8], cooperative effects [9] and nano-optomechanics [10]. Optical nanofibers (ONFs) with subwavelength diameters are considered potential candidates to realize all-fiber structures due to their versatility for these applications. This platform is extensible as an interface to couple quantum emitters, in which efficient coupling can be realized. The quantum emitters in the vicinity of an ONF can be coherently manipulated and interrogated using guided light [11–14]. A theoretical proposal predicts that a significant fraction of spontaneous emission by an atom near ONFs can be effectively channeled into guided modes [11], and this behavior has been demonstrated [15]. Additionally, one-dimensional single atomic arrays can be prepared using the evanescent field of the ONF [16,17]. Electromagnetically induced transparency and long-term storage in ONFs have been demonstrated experimentally [18,19]. Precise measurement methods have been implemented in an ONF-atom system to realize diverse measurement applications of atomic dynamics [20–22]. The collective effects of single atoms coupled to the ONF have also been studied, such as atomic mirrors [23,24], super/subradiation [25], and collective emission at the single-photon level [26]. Furthermore, an ONF as a high-transmission waveguide can mediate single atoms separated for long distances, which paves the way for many-body physics [4–27].

#420243 https://doi.org/10.1364/OE.420243
Journal © 2021 Received 19 Jan 2021; revised 27 Feb 2021; accepted 18 Mar 2021; published 25 Mar 2021

Optics EXPRESS

The reason for the high coupling efficiency of ONFs is that ONFs with ultrathin waists at the subwavelength level can offer a strong transverse confinement of the guided modes, which leads to the spread of a powerful evanescent field surrounding the ONFs [28]. If a single quantum emitter (SQE) overlaps with the evanescent field, then considerable fluorescence from the SQE can be channeled into the ONF [12]. The guided fluorescence can propagate along the fiber, which is more convenient than conventional free-space coupling using a high-aperture lens [29] with bulky configurations. Moreover, ONFs can be integrated easily with other fiber systems or micro/nanostructures.

In recent years, researchers have made efforts to precisely control the position of SQEs or arrays and to prove the coupling between ONFs and SQEs. For a typical ONF, the SQE can only be placed on the surface of the ONF. The coupling efficiency between a silica ONF and an SQE depends on the relation of $kd = 2 \times 1.45$, where k is the wavenumber of the SQE and d is the ONF diameter. With a proper ONF diameter, the coupling efficiency can be up to 20%-30% due to the strong transverse confinement of the ONF [11]. To enhance the coupling efficiency based on ONFs, more schemes and experiments have been proposed and demonstrated. High coupling efficiency can be achieved by confining the guided light along the ONF axis, namely, cavity enhancements [30–32]. Thanks to the well-established technologies of micro/nanofabrication, ONFs can be tailored, and the coupling efficiency can be substantially enhanced [33–35]. Various tailored ONFs with complicated structures have been proposed [36–42]. It is expected that the coupling efficiency exhibits the potential to reach 80% or more [34]. Experiments with solid-state quantum emitters and cold atoms have been accomplished, in which remarkable enhancements are demonstrated [15,43–47]. All the above mentioned proposals and experiments show great improvement in the coupling efficiency between ONFs and SQEs on the surface of ONFs. Nevertheless, ONFs with complicated structures for cavity enhancement can increase experimental difficulties, which is still a challenge. In addition, the more complicated periodical structures are not easy to characterize unambiguously, which concerns optimizing the parameters of periodical structures. Tradeoffs between high coupling efficiency and simple configurations are crucial for experiments.

To enhance the coupling efficiency, it was proposed that the coupling efficiency can be improved up to 53.4% when an SQE is placed inside the body of an ONF [48]; however, this structure cannot be conveniently realized experimentally. To place the SQEs into ONFs, a narrow air-filled groove in an ONF with a cavity grating was proposed, with a coupling efficiency reaching 80% [49]. This great enhancement is due to both the cavity grating and the narrow groove because the cavity grating and the air-filled groove embedded in the ONF induce a strong local field enhancement.

In this paper, we propose a simple scheme to enhance the coupling efficiency of an SQE using an ONF with only one hole embedded along the ONF radial axis. When the SQE is inside the hole, the coupling efficiency for different SQE positions and polarizations is studied. For this simple structure, there is a significant enhancement of the coupling efficiency. Experimentally, it is achievable and convenient to place an SQE in the hole. The simulation results show that the coupling efficiency can reach 62.8% when a single quantum emitter with azimuthal polarization is at a position 200 nm from the middle of the hole along the hole-axial direction. The diameters of the ONF and the hole are 800 nm and 400 nm, respectively, while the wavelength of the single quantum emitter is 852 nm. The coupling efficiency can be optimized by setting appropriate diameters of the ONF and the hole. This proposal of enhancing the coupling efficiency using a hole-tailored ONF has great potential for applications such as small particle detection, quantum information processing and quantum precision measurements.

Optics EXPRESS

2. Numerical simulations

Figure 1(a) schematically shows the illustrations of a normal ONF for coupling an SQE in the vicinity of the ONF. The finite difference time domain (FDTD) method is used for numerical simulations to obtain the coupling efficiency of the SQEs. In Fig. 1(a), for a normal ONF, the SQE is placed on the surface of the ONF. The wavelength of SQE is 852 nm. We simulate and plot the coupling efficiency as a function of the ONF diameter between the ONF and the SQE, as shown in Fig. 1(b). A fraction of up to 31.6% of photons emitted by the SQE with radial polarization are coupled into the ONF guided modes. A 20.5% coupling efficiency for azimuthal polarization and a 9.8% coupling efficiency for axial polarization are achieved. The average coupling efficiency for the three polarizations is 20.6%, which agrees with previous work [11].

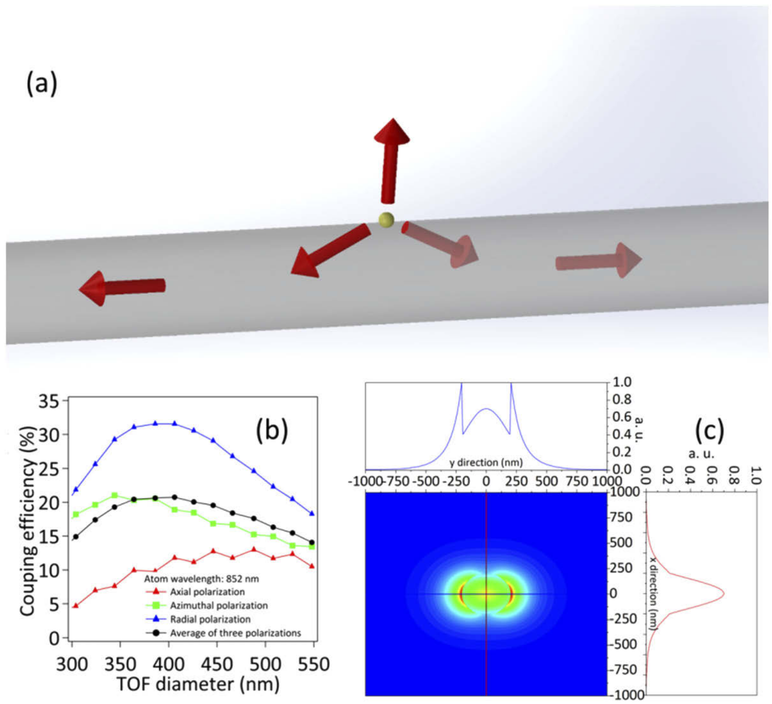

Fig. 1. (a) Diagram of the coupling system based on the normal ONF. A single quantum emitter with a wavelength of 852 nm is placed on the surface of the ONF. The figure is not drawn to scale. (b) Coupling efficiencies corresponding to different ONF diameters are calculated. (c) Electric field intensity transverse distribution of the guided mode in the ONF, where TE and TM modes are degenerate.

Due to the modification of the vacuum caused by the ONF, the coupling between the ONF and the SQE can be expressed by $H = d \cdot E_{total} = (E_{guided} + E_{radiation})$ [11], where d is dipole operator of the SQE, E_{total} is the total electric field which can be decomposed into guided mode E_{guided} and radiation mode $E_{radiation}$ components. The H can directly determine the spontaneous rate of the SQE, where they also can be divided into two parts as $\gamma_{\text{total}} = \gamma_{guided} + \gamma_{radiation}$. Here,

$$\gamma_{guided} = \frac{2\omega_0 \beta_0{}'}{\varepsilon_0 \hbar} \sum_g |(d_{eg} \cdot e^{(\omega_0,+,+)})|^2 \tag{1}$$

$$\gamma_{radiation} = \frac{2\omega_0}{\varepsilon_0 \hbar} \sum_g \sum_m \int_0^{k_0 n_2} d\beta |(d_{eg} \cdot e^{(\omega_0,\beta,m,+)})|^2 \tag{2}$$

Optics EXPRESS

where ω_0 is the frequency of photons, β is the longitudinal propagation constant, β' is the derivative of β with respect to ω_0, e, g represent the excited state and ground state of hyper-fine structure respectively while m is the sublevel. The $(\omega_0, +, +)$ denotes the frequency, forward propagation direction and counterclockwise rotation of polarization respectively.

The coupling efficiency of an SQE coupled into an ONF is defined as $\beta = \gamma_{guided}/\gamma_{total}$. In the FDTD simulations, the coupling efficiency is defined as $\beta = \gamma_{guided}/\gamma_{total} = 2P_{guided}T/P_{emitter} = C$, where γ_{guided} is the power of the fluorescence coupled into guided mode, $P_{emitter}$ is the total power of the fluorescence from the SQE, and T is the transmission of the ONF. The "2" in the numerator indicates the coupling efficiency of both sides of the ONF. Actually, the ONF can enhance the spontaneous emission rate of the SQE, which is expressed by the Purcell factor of $PF = \gamma_{total}/\gamma_0$, where γ_0 represents the spontaneous emission rate in free space. The total collected fluorescence is determined by both of the Purcell factor and coupling efficiency.

To enhance the coupling efficiency, we propose a simple photonic structure-hole-tailored ONF. Figure 2(a) shows a hole-tailored ONF for enhancing the coupling efficiency of an SQE. The ONF is tailored with a hole, and the hole penetrates the ONF along the radial axis of the ONF. The ONF axis is defined as the z-axis. The hole axis is defined as y-axis. The coordinate origin is the center of the hole, which is on the ONF axis simultaneously. The hole restructures the electric field intensity transversal distribution of the guided mode in the ONF, as shown in Fig. 2(b) and (c) for the TE mode and TM mode, respectively. The ONF diameter is 800 nm, and the diameter of the hole is 400 nm. The wavelength of the guided modes is 852 nm.

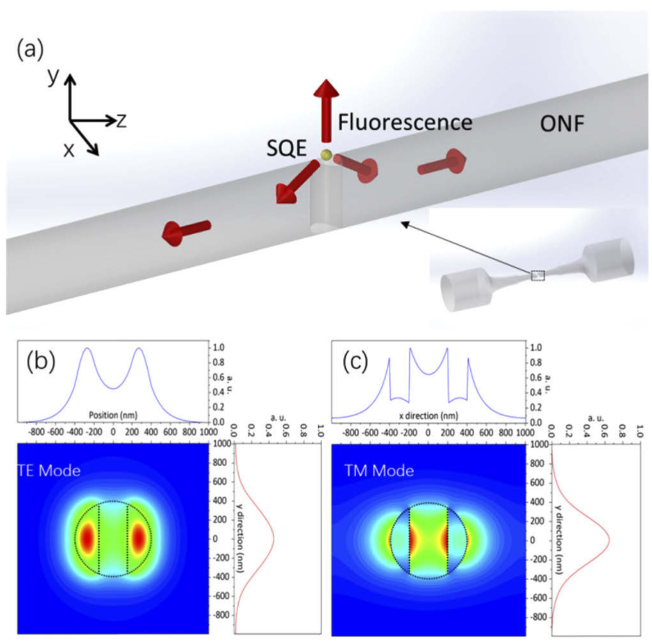

Fig. 2. (a) Diagram of the hole-tailored ONF for enhancing the coupling efficiency of an SQE (yellow balls). The SQE is placed in the hole. Inset shows the full schematic of the tailored ONF. The figures are not drawn to scale. (b) and (c) show the electric field intensity transverse distribution of the guided mode in the ONF. (b) TE mode and (c) TM mode in the ONF. The diameters of the ONF and hole are 800 nm and 400 nm, respectively, and the SQE wavelength is 852 nm.

In the hole-tailored ONF, the electric field in the hole (Fig. 2(c)) shows much stronger confinement of light than normal ONF (Fig. 1(c)) [41,49]. The hole-tailored ONF with a small volume mode leads to a high-intensity distribution of the electric filed, therefore we can

Optics EXPRESS

explain why the coupling efficiency can be significantly enhanced. In addition, the electric field distribution is spatially variable. If an SQE is placed into the hole, then a maximum of the coupling efficiency can be found when the position of the SQE is scanned spatially.

The SQE is placed in the axis of the hole, and its position along the axis of the hole (y-axis) is scanned. The coupling efficiencies as a function of y are shown in Fig. 3. Figures 3(a)-(c) shows the coupling efficiencies of the axial (z), radial (y) and azimuthal (x) polarizations of the SQE. In this case, the hole diameter varies from 50 nm to 350 nm, and the ONF diameter is 400 nm. Figures 3(d)-(f) shows the case when the hole diameter changes from 50 nm to 550 nm and the ONF diameter is 600 nm. Figures 3(g)-(i) shows the case when the hole diameter varies from 100 nm to 700 nm and the ONF diameter is 800 nm.

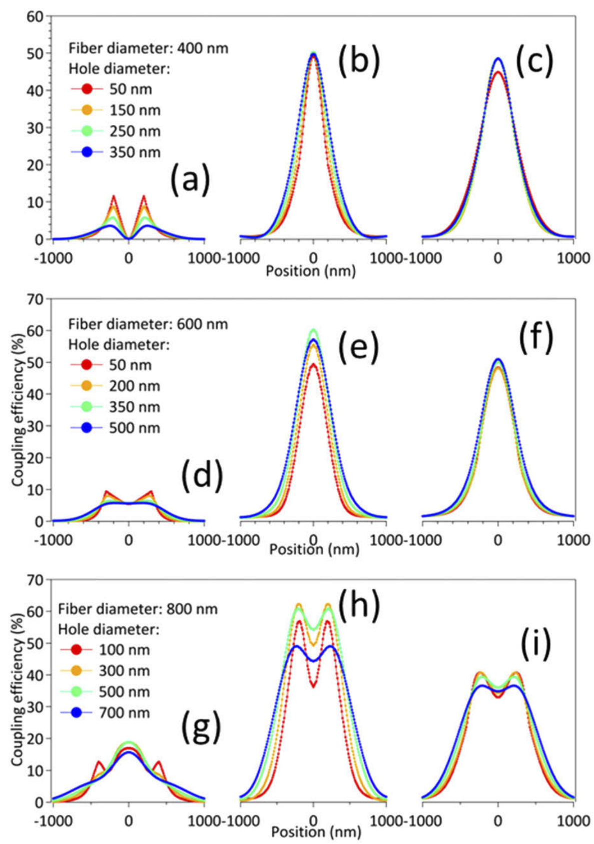

Fig. 3. Coupling efficiency as a function of the SQE position along the y-axis. (a-c), (d-f) and (g-i) show the cases with ONF diameters of 400, 600 and 800 nm, respectively. From left to right of each figure group shows the axial, azimuthal and radial polarizations of the SQE. Different hole diameters are simulated in each figure. For each case, the hole diameters for the four values are shown.

From Fig. 3, we find that the SQE's position with respect to the maximum coupling efficiency is no longer in the middle of the hole as the SQE is scanned over the entire hole along the y-axis. There are two optimum positions that are at a quarter of the ONF diameter from the middle point. Identical phenomena occur with the azimuthal and radial polarizations. That can also be explained by the dependence of the coupling efficiency on E_{guided}.

The coupling efficiency between the hole-tailored ONF and the SQE depends on the entire structure of the ONF and the position of the SQE. Qualitatively, the coupling efficiency can be

Optics EXPRESS

effected strongly by the volume ratio of the Silica structure and the free space around the SQE. This is easy to understand from the case of a normal ONF with a SQE on its surface. The ratio of the Silica structure and the free space only depends on the diameter of the ONF. Figure 1(b) has shown that there exists an optimal ONF diameter for maximum coupling efficiency. For the case of a SQE inside the hole of a tailored ONF, the ratio depends on the volume of the Silica around the SQE. Bigger or smaller volume ratio results in the decrease of coupling efficiency. When the ONF diameter is small, the center of the hole is the best position for the coupling efficiency. When the ONF diameter is big enough, the coupling efficiency of the center of the hole decreases because of the big volume ratio. However, the volume ratio decreases when SQE moves away from the center of hole, and the coupling efficiency would increase and reach maximum. When SQE moves more, the coupling efficiency decreases due to the decreasing volume ratio. Because of the symmetrical structure of the hole-tailored ONF, there exists two optimum positions on the both side of the hole center. From Fig. 3(g)-(i) we find that optimal positions are almost invariable with different hole diameters for a fixed ONF diameter. We can find a cut-off ONF diameter if the hole diameter is constant. When the ONF diameter is samller than the cut-off diameter, the optimal position is the center of the hole. When the ONF diameter is larger than the cut-off diameter, the optimal position splits into two and the positions move away from the center of ONF as increasing ONF diameter. We simulate the cut-off ONF diameter as a function of the SQE wavelength, and the results are shown in Fig. 4(b). The relation is linear. The hole diameter satisfies the relation of $d = 1.45\lambda/\pi$

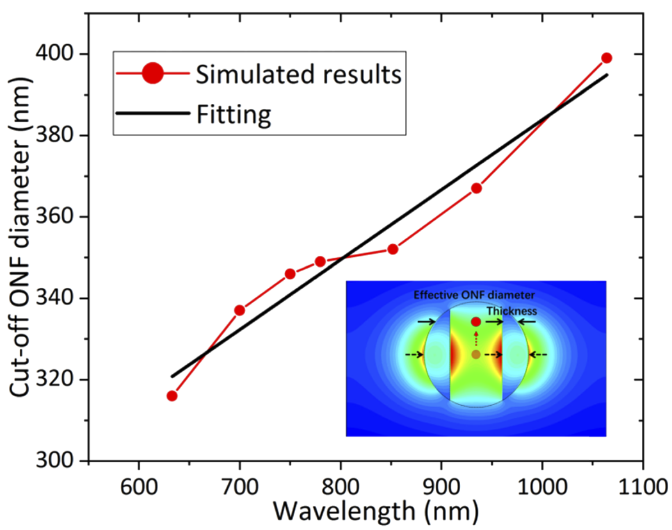

Fig. 4. Cut-off ONF diameter as a function of wavelength, which is represented by red solid dot. The black line is linear fitting. The SQE polarization is along the x-axis. Inset shows the diagram of the SQE moving through the hole. We scan the position of the SQE to find the optimal cut-off ONF diameter. The volme ration changes as the SQE's position.

Here we would like to state again that the optimal coupling efficiency is determined by the entire structure of the hole-tailored ONF. For this complex structure, it is not easy to analyze quantitatively, hence we give a qualitative explanation for the simulation results.

Finally, we find that the optimized configuration is obtained when the hole diameter is 400 nm and the ONF diameter is 800 nm (Fig. 3(h)). The Purcell factor of this configuration as a function of the SQE position along y axis for different polarizations are shown in Fig. 5. Additionally, the maximum coupling efficiency is 62.8%, and the SQE's position is $y = \pm 200nm$.

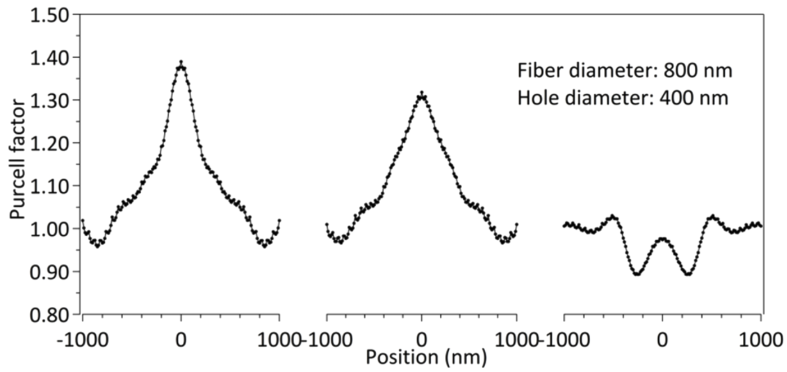

Fig. 5. Purcell factor as a function of the SQE position along the y-axis. From left to right of each figure shows the axial, azimuthal and radial polarizations of the SQE. The ONF diameter is 800 nm and the hole diamter is 400 nm.

Then, to find the global optimum SQE position, we further scan the position of the SQE along the z-axis and x-axis when the SQE position is $y = -200nm$. The corresponding coupling efficiencies versus different polarizations and the average values are shown in Fig. 6. The results indicate that the maximum coupling efficiency is obtained when the SQE is in the middle of the hole along the x, z-axis, and the average coupling efficiency decreases monotonically as the SQE approaches the ONF wall. For z-axis scanning, the coupling efficiency changes gently, but the maximum is also in the middle of the hole. This finding confirms that the two positions with $(x, y, z) = (0, 0, \pm 200nm)$ are the optimal positions where the highest coupling efficiency of the fluorescence emitted from the SQE is achieved.

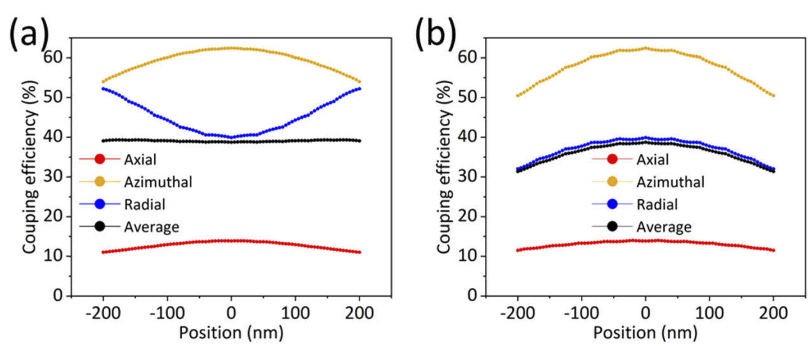

Fig. 6. Coupling efficiency as a function of the SQE position scanning along the z-axis (a) and x-axis (b) when y=-200 nm.

Based on the simulation results from Fig. 3 and Fig. 6, we conclude that the optimized coupling efficiency is a function of the hole diameter with ONF diameters of 400 nm, 600 nm and 800 nm, as shown in Fig. 7. The lowest coupling efficiency is always obtained for the axial polarization of the SQE, while the azimuthal polarization corresponds to the highest coupling efficiency. The best configuration of hole-tailored ONF is that the ONF diameter is 800 nm with a hole diameter of 400 nm. We find that the maximum coupling efficiency for the azimuthal polarization (x direction) can reach 62.8%. The coupling efficiency can reach 39% for the average of the three polarizations. This result is two times that of the case of the ONF without a tailored hole (shown in Fig. 1).

Optics EXPRESS

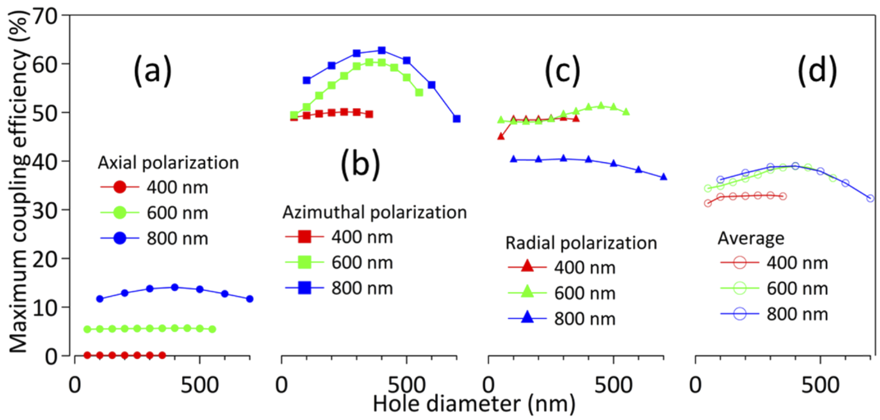

Fig. 7. Maximum coupling efficiency as a function of the hole diameter. The red, green and blue lines represent the different ONF diameters corresponding to 400 nm, 600 nm and 800 nm, respectively. (a), (b), and (c) represent the axial, azimuthal, and radial polarizations of the SQE, respectively, and (d) is their average.

Afterwards, the cases for larger ONF diameters are also investigated, and the maximum coupling efficiencies for all cases can still be obtained when the hole diameter is 400 nm, regardless of the ONF diameter when the SQE wavelength is 852 nm. After that, to find the optimum hole diameter for different SQE wavlength, we simulate to maximum coupling efficiency as a funciton of the SQE wavelength when the ONF diameter is fixed at 800 nm. The simulation results is shown in Fig. 8. The hole diameter should be larger to get maixmum coupling efficiency when SQE wavelength increases. We infer that the relation between the hole diameter and the wavelength can be explained by the linear dependence of $d = n\lambda/\pi$ [11], where d is the ONF diameter and n is the refractive index which is set to be 1.45 here constantly.

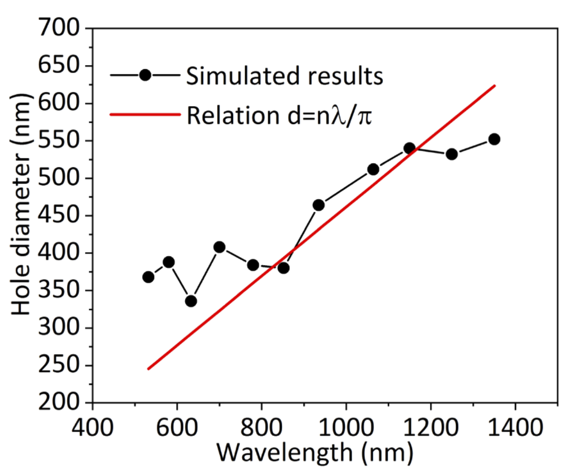

Fig. 8. Hole diameter for maximum coupling efficiency as a function of the SQE wavelength. The ONF diameter is fixed at 800 nm. Black dots show the simulated results and red line shows the relation $d = n\lambda/\pi$, where n is set to be 1.45 constantly.

Regarding to the mesh size, they are constant in our calculations. The minimum mesh step is 0.25 nm, and the minimum evolution time is 0.01 fs, which are much smaller than the scales of the simulation field. This is small enough and has no effect on the simulation results. We

Optics EXPRESS

infer that the fluctuations are due to two reasons. The first one is that the fixed ONF diameter for different SQE wavelength. Because the best coupling efficiency depends on the three parameters including SQE wavelength, ONF diameter and hole diameter. When the SQE wavelength and hole diameter are scanned, the corresponding optimal ONF diameter will fluctuate, even though the fluctuations are small. However, in Fig. 6 (Fig. 8 in revised manuscript) the ONF diameter is a constant of 800 nm, which results in the fluctuations. The second reason is that the refractive index of hole-tailored ONF changes with the SQE wavelength, which will affect the simulation results and cause fluctuations.

3. Conclusions

Owing to the micro/nanofabrication technique, such structures can be fabricated by focused ion beams (FIBs) with high precision. Versatile similar structures obtained by tailoring the ONF with an FIB have been proposed [41,49,50], and some of them have been fabricated experimentally [51,52]. Besides, this structure is also promising in trapping single atoms, since the related proposal has been introduced in [53]. In this reference, the surrounding two-dimensional Van der Waals potential field generated by the hole wall can be counteracted by blue-detuned guided mode and the three-dimensional confinement of the trap can be further realized by the combination of the blue-detuned and red-detuned guided modes. In our manuscript, the hole-tailored ONF is similar to the slot-cut nanostructure in this reference. The hole-tailored ONF has the similar transversal guided modes, see Fig. 2(b) and (c) in our manuscript. We can use the similar method to trap single atoms in the hole-tailored ONF, while the single atoms are located in the middle of the optimal positions. Based the results of the reference mentioned above, we can infer the position fluctuation of the SQE trapped in the trap formed by a hole-tailored ONF is around tens of nanometers when the trap depth of is over 1 mK and the temperature of the SQE is around 20μK. The coupling efficiency between single atoms and the hole-tailored ONF in vicinity of the optimal positions changes gently, see Fig. 3(g)-(i) and Fig. 6, the variation of the coupling efficiency is estimated to be lower than 5%. For these reasons, we believe that the photons emitted from the trapped atom can be coupled into the hole-tailored ONF with a high coupling efficiency. Hence our proposal is realizable, and it is also significant for further studies on more complicated periodic structures [41].

In conclusion, we have proposed a hole-tailored ONF to enhance the coupling efficiency between the ONF and an SQE. We have determined the appropriate parameters for the ONF and the hole based on the simulation results. Under the optimal parameters at an SQE wavelength of 852 nm, the maximum coupling efficiency can reach 62.8% for the azimuthal polarization of SQE and 39% for an average of three polarizations when the ONF diameter and the hole diameter are 800 nm and 400 nm, respectively. We find that in optimal configuration, there exists two optimal positions, which can provide an extra optimal site in experiment for higher average coupling efficiency in experiment, in addition, the two sites are promising to interact with each other. This scheme is simple, and the enhanced coupling is easily two times that of an ONF without a tailored hole. Additionally, the coupling efficiency between the ONF and the SQE is improved significantly. The fundamental calculations based on the simple model are also of importance in extending it to a tailored periodic array for large-scale integrated quantum internet. This structure can be fabricated by micro/nanofabrication technologies with high precision. These fabrication technologies have undergone long-term development during the past few years. SQEs can be efficiently interfaced with hole-tailored ONFs and have great potential for applications in quantum information processing and quantum precision measurements.

Funding. National Key Research and Development Program of China (2017YFA0304502); National Natural Science Foundation of China (11634008, 11974223, 11974225); the Fund for Shanxi "1331 Project" Key Subjects.

Disclosures. The authors declare that there are no conflicts of interest related to this article.

Optics EXPRESS

References

1. H. J. Kimble, "The quantum internet," Nature **453**(7198), 1023–1030 (2008).
2. J. P. Reithmaier, G. Sęk, A. Löffler, C. Hofmann, S. Kuhn, S. Reitzenstein, L. V. Keldysh, V. D. Kulakovskii, T. L. Reinecke, and A. Forchel, "Strong coupling in a single quantum dot–semiconductor microcavity system," Nature **432**(7014), 197–200 (2004).
3. R. Chikkaraddy, B. de Nijs, F. Benz, S. J. Barrow, O. A. Scherman, E. Rosta, A. Demetriadou, P. Fox, O. Hess, and J. J. Baumberg, "Single-molecule strong coupling at room temperature in plasmonic nanocavities," Nature **535**(7610), 127–130 (2016).
4. D. H. White, S. Kato, N. Német, S. Parkins, and T. Aoki, "Cavity Dark Mode of Distant Coupled Atom-Cavity Systems," Phys. Rev. Lett. **122**(25), 253603 (2019).
5. K. P. Nayak and K. Hakuta, "Nanofiber quantum photonics," J. Opt. **20**(7), 073001 (2018).
6. X. Ding, Y. He, Z.-C. Duan, N. Gregersen, M.-C. Chen, S. Unsleber, S. Maier, C. Schneider, M. Kamp, S. Höfling, C.-Y. Lu, and J.-W. Pan, "On-Demand single photons with high extraction efficiency and Near-Unity indistinguishability from a resonantly driven quantum dot in a micropillar," Phys. Rev. Lett. **116**(2), 020401 (2016).
7. D. E. Chang, A. S. Srensen, E. A. Demler, and M. D. Lukin, "A single-photon transistor using nanoscale surface plasmons," Nat. Phys. **3**(11), 807–812 (2007).
8. R. E. Evans, M. K. Bhaskar, D. D. Sukachev, C. T. Nguyen, A. Sipahigil, M. J. Burek, B. Machielse, G. H. Zhang, A. S. Zibrov, E. Bielejec, H. Park, M. Loncar, and M. D. Lukin, "Photon-mediated interactions between quantum emitters in a diamond nanocavity," Science **362**(6415), 662–665 (2018).
9. S. Putz, D. O. Krimer, R. Amsüss, A. Valookaran, T. Nöbauer, J. Schmiedmayer, S. Rotter, and J. Majer, "Protecting a spin ensemble against decoherence in the strong-coupling regime of cavity QED," Nat. Phys. **10**(10), 720–724 (2014).
10. M. Aspelmeyer, T. J. Kippenberg, and F. Marquardt, "Cavity optomechanics," Rev. Mod. Phys. **86**(4), 1391–1452 (2014).
11. F. L. Kien, S. Dutta Gupta, V. I. Balykin, and K. Hakuta, "Spontaneous emission of a cesium atom near a nanofiber: Efficient coupling of light to guided modes," Phys. Rev. A **72**(3), 032509 (2005).
12. K. P. Nayak, P. N. Melentiev, M. Morinaga, F. L. Kien, V. I. Balykin, and K. Hakuta, "Optical nanofiber as an efficient tool for manipulating and probing atomic fluorescence," Opt. Express **15**(9), 5431 (2007).
13. K. P. Nayak and K. Hakuta, "Single atoms on an optical nanofibre," New J. Phys. **10**(5), 053003 (2008).
14. D. Manoj, A. Shirasaki, K. P. Nayak, M. Morinaga, F. L. Kien, and K. Hakuta, "Measurement of fluorescence emission spectrum of few strongly driven atoms using an optical nanofiber," Opt. Express **18**(16), 17154–17164 (2010).
15. R. Yalla, M. Sadgrove, K. P. Nayak, and K. Hakuta, "Cavity quantum electrodynamics on a nanofiber using a composite photonic crystal cavity," Phys. Rev. Lett. **113**(14), 143601 (2014).
16. E. Vetsch, D. Reitz, G. Sague, R. Schmidt, S. T. Dawkins, and A. Rauschenbeutel, "Optical interface created by laser-cooled atoms trapped in the evanescent field surrounding an optical nanofiber," Phys. Rev. Lett. **104**(20), 203603 (2010).
17. A. Goban, K. S. Choi, D. J. Alton, D. Ding, C. Lacroute, M. Pototschnig, T. Thiele, N. P. Stern, and H. J. Kimble, "Demonstration of a state-insensitive, compensated nanofiber trap," Phys. Rev. Lett. **109**(3), 033603 (2012).
18. B. Gouraud, D. Maxein, A. Nicolas, O. Morin, and J. Laurat, "Demonstration of a memory for tightly guided light in an optical nanofiber," Phys. Rev. Lett. **114**(18), 180503 (2015).
19. C. Sayrin, C. Clausen, B. Albrecht, P. Schneeweiss, and A. Rauschenbeutel, "Storage of fiberguided light in a nanofiber-trapped ensemble of cold atoms," Optica **2**(4), 353–356 (2015).
20. J.-B. Béguin, E. M. Bookjans, S. L. Christensen, H. L. Sørensen, J. H. Müller, E. S. Polzik, and J. Appel, "Generation and detection of a Sub-Poissonian atom number distribution in a One-Dimensional optical lattice," Phys. Rev. Lett. **113**(26), 263603 (2014).
21. J. A. Grover, P. Solano, L. A. Orozco, and S. L. Rolston, "Photon-correlation measurements of atomic-cloud temperature using an optical nanofiber," Phys. Rev. A **92**(1), 013850 (2015).
22. A. Dareau, Y. Meng, P. Schneeweiss, and A. Rauschenbeutel, "Observation of ultrastrong Spin-Motion coupling for cold atoms in optical microtraps," Phys. Rev. Lett. **121**(25), 253603 (2018).
23. H. L. Sorensen, J. B. Beguin, K. W. Kluge, I. Iakoupov, A. S. Sorensen, J. H. Muller, E. S. Polzik, and J. Appel, "Coherent backscattering of light off one-dimensional atomic strings," Phys. Rev. Lett. **117**(13), 133604 (2016).
24. N. V. Corzo, B. Gouraud, A. Chandra, A. Goban, A. S. Sheremet, D. Kupriyanov, and J. Laurat, "Large bragg reflection from one-dimensional chains of trapped atoms near a nanoscale waveguide," Phys. Rev. Lett. **117**(13), 133603 (2016).
25. P. Solano, P. Barberis-Blostein, F. K. Fatemi, L. A. Orozco, and S. L. Rolston, "Super-radiance reveals infinite-range dipole interactions through a nanofiber," Nat. Commun. **8**(1), 1857 (2017).
26. N. V. Corzo, J. Raskop, A. Chandra, A. S. Sheremet, B. Gouraud, and J. Laurat, "Waveguide-coupled single collective excitation of atomic arrays," Nature **566**(7744), 359–362 (2019).
27. S. Kato, N. Német, K. Senga, S. Mizukami, X. Huang, S. Parkins, and T. Aoki, "Observation of dressed states of distant atoms with delocalized photons in coupled-cavities quantum electrodynamics," Nat. Commun. **10**(1), 1160 (2019).

Optics EXPRESS

28. F. L. Kien, J. Q. Liang, K. Hakuta, and V. I. Balykin, "Field intensity distributions and polarization orientations in a vacuum-clad subwavelength-diameter optical fiber," Opt. Commun. **242**(4-6), 445–455 (2004).
29. M. K. Tey, Z. L. Chen, S. A. Aljunid, B. Chng, F. Huber, G. Maslennikov, and C. Kurtsiefer, "Strong interaction between light and a single trapped atom without the need for a cavity," Nat. Phys. **4**(12), 924–927 (2008).
30. M. Sadgrove, R. Yalla, K. P. Nayak, and K. Hakuta, "Photonic crystal nanofiber using an external grating," Opt. Lett. **38**(14), 2542–2545 (2013).
31. P. Schneeweiss, S. Zeiger, T. Hoinkes, A. Rauschenbeutel, and J. Volz, "Fiber ring resonator with a nanofiber section for chiral cavity quantum electrodynamics and multimode strong coupling," Opt. Lett. **42**(1), 85–88 (2017).
32. F. Cheng, P. F. Zhang, X. Wang, and T. C. Zhang, *J. Quantum Opt.* 23(1), 74–81 (2017).
33. J. T. Robinson, C. Manolatou, L. Chen, and M. Lipson, "Ultrasmall mode volumes in dielectric optical microcavities," Phys. Rev. Lett. **95**(14), 143901 (2005).
34. F. L. Kien and K. Hakuta, "Cavity-enhanced channeling of emission from an atom into a nanofiber," Phys. Rev. A **80**(5), 053826 (2009).
35. H. Takashima, M. Fujiwara, A. W. Schell, and S. Takeuchi, "Detailed numerical analysis of photon emission from a single light emitter coupled with a nanofiber Bragg cavity," Opt. Express **24**(13), 15050–15058 (2016).
36. K. P. Nayak, F. L. Kien, Y. Kawai, K. Hakuta, K. Nakajima, H. T. Miyazaki, and Y. Sugimoto, "Cavity formation on an optical nanofiber using focused ion beam milling technique," Opt. Express **19**(15), 14040–14050 (2011).
37. C. Wuttke, M. Becker, S. Brückner, M. Rothhardt, and A. Rauschenbeutel, "Nanofiber Fabry–Perot microresonator for nonlinear optics and cavity quantum electrodynamics," Opt. Lett. **37**(11), 1949–1951 (2012).
38. K. P. Nayak and K. Hakuta, "Photonic crystal formation on optical nanofibers using femtosecond laser ablation technique," Opt. Express **21**(2), 2480–2490 (2013).
39. T. G. Tiecke, K. P. Nayak, J. D. Thompson, T. Peyronel, N. P. de Leon, V. Vuletić, and M. D. Lukin, "Efficient fiber-optical interface for nanophotonic devices," Optica **2**(2), 70–75 (2015).
40. Y. Sun, Y. Yu, H. Liu, Z. Li, and W. Ding, "Optical microfiber-based photonic crystal cavity," J. Phys.: Conf. Ser. **680**, 012029 (2016).
41. W. Li, J. Du, V. G. Truong, and S. N. Chormaic, "Optical nanofiber-based cavity induced by periodic air-nanohole arrays," Appl. Phys. Lett. **110**(25), 253102 (2017).
42. P. F. Zhang, G. Li, and T. C. Zhang, "Subwavelength optical dipole trap for neutral atoms using a microcapillary tube tip," J. Phys. B: At., Mol. Opt. Phys. **50**(4), 045005 (2017).
43. R. N Patel, T. Schröder, N. Wan, L. Li, S. L. Mouradian, E. H. Chen, and D. R. Englund, "Efficient photon coupling from a diamond nitrogen vacancy center by integration with silica fiber," Light: Sci. Appl. **5**(2), e16032 (2016).
44. C. Junge, D. O'Shea, J. Volz, and A. Rauschenbeutel, "Strong Coupling between single atoms and nontransversal Photons," Phys. Rev. Lett. **110**(21), 213604 (2013).
45. S. Kato and T. Aoki, "Strong coupling between a trapped single atom and an all-fiber cavity," Phys. Rev. Lett. **115**(9), 093603 (2015).
46. D. E. Jones, G. T. Hickman, J. D. Franson, and T. B. Pittman, "Nanofiber-segment ring resonator," Opt. Lett. **41**(16), 3683–3685 (2016).
47. S. K. Ruddell, K. E. Webb, I. Herrera, A. S. Parkins, and M. D. Hoogerland, "Collective strong coupling of cold atoms to an all-fiber ring cavity," Optica **4**(5), 576–579 (2017).
48. M. Almokhtar, M. Fujiwara, H. Takashima, and S. Takeuchi, "Numerical simulations of nanodiamond nitrogen-vacancy centers coupled with tapered optical fibers as hybrid quantum nanophotonic devices," Opt. Express **22**(17), 20045–20059 (2014).
49. W. F. Li, J. J. Du, and S. N. Chormaic, "Tailoring a nanofiber for enhanced photon emission and coupling efficiency from single quantum emitters," Opt. Lett. **43**(8), 1674–1677 (2018).
50. F. L. Kien, K. P. Nayak, and K. Hakuta, "Nanofibers with Bragg gratings from equidistant holes," J. Mod. Opt. **59**(3), 274–286 (2012).
51. J. D. Thompson, T. G. Tiecke, N. P. de Leon, J. Feist, A. V. Akimov, M. Gullans, A. S. Zibrov, V. Vuletić, and M. D. Lukin, "Coupling a Single Trapped Atom to a Nanoscale Optical Cavity," Science **340**(6137), 1202–1205 (2013).
52. A. Goban, C.-L. Hung, S.-P. Yu, J. D. Hood, J. A. Muniz, J. H. Lee, M. J. Martin, A. C. McClung, K. S. Choi, D. E. Chang, O. Painter, and H. J. Kimble, "Atom–light interactions in photonic crystals," Nat. Commun. **5**(1), 3808 (2014).
53. M. Daly, V. G. Truong, C. F. Phelan, K. Deasy, and S. Nic Chormaic, "Nanostructured optical nanofibres for atom trapping," New J. Phys. **16**(5), 053052 (2014).